

# Mapping a fracture network formed by hydraulic fracturing in a shale gas reservoir

Elżbieta Węglińska<sup>1</sup>, Andrzej Leśniak<sup>2</sup>, Andrzej Pasternacki<sup>3</sup>, Paweł Wandycz<sup>4</sup>

<sup>1</sup> AGH University of Krakow, Faculty of Geology, Geophysics and Environmental Protection, Department of Geoinformatics and Applied Computer Science, Krakow, Poland, e-mail: weglinska@agh.edu.pl (corresponding author), ORCID ID: 0000-0003-0645-6570

<sup>2</sup> AGH University of Krakow, Faculty of Geology, Geophysics and Environmental Protection, Department of Geoinformatics and Applied Computer Science, Krakow, Poland, ORCID ID: 0000-0002-9442-0799

<sup>3</sup> AGH University of Krakow, Poland, Faculty of Geology, Geophysics and Environmental Protection, Department of Energy Resources, Krakow, Poland, ORCID ID: 0000-0002-0934-0277

<sup>4</sup> AGH University of Krakow, Faculty of Geology, Geophysics and Environmental Protection, Department of Energy Resources, Krakow, Poland, ORCID ID: 0000-0002-1145-0184

© 2024 Author(s). This is an open access publication, which can be used, distributed and re-produced in any medium according to the Creative Commons CC-BY 4.0 License requiring that the original work has been properly cited.

Received: 24 November 2023; accepted: 8 June 2024; first published online: 21 June 2024

**Abstract:** Microseismic monitoring is an important technique that can be used to identify fractures in rock mass. The aim of this article is to identify, on the basis of the location of microseismic events, structures formed by hydraulic fracturing in the Wysin-2H/2Hbis horizontal well from the Baltic Basin in northern Poland, and to compare the patterns of these structures with the direction of regional stresses. The authors proposed a novel multi-step workflow for finding these structures. To be able to delineate the structures from microseismic events with greater accuracy, a collapsing algorithm was used. Then, based on the Hierarchical Density-Based Spatial Clustering of Applications with Noise (HDBSCAN) clustering algorithm and the elongation coefficient of each cluster, probable fissures were identified and compared against the maximum horizontal stress direction. In addition, based on the 3D seismic data from the Wysin and the calculated geomechanical parameters in the monitoring well, the probability classes of brittleness indices in the LMR ( $\lambda\rho-\mu\rho$ ) parameter domain were determined. A comparative analysis was performed between the two variants of microseismic event location (before and after the collapsing procedure) and the estimated probability of a given class of brittleness index. The comparison of the event location with the 3D seismic data was used to validate the results before and after collapsing due to the high resolution of the seismic method. It is shown that the collapsed events appeared in more rigid regions, where more energy release is expected.

**Keywords:** fracture network, shale gas, microseismicity, collapsing, HDBSCAN, Baltic Basin

## INTRODUCTION

Hydraulic fracturing (HF) is a technique that allows fractures to be created in a rock formation to stimulate the flow of oil or gas. This process

is carried out by pumping fracturing fluid under high pressure into a well to create new fractures or enlarge pre-existing fractures in the rock. Creation of hydraulic fractures or reactivation of existing fractures by hydraulic stimulation induces

microseismic events (Maxwell 2013). Based on the location of microseismic events, it is possible to identify fractures in the rock mass. Fracture mapping is key to estimating stimulation effectiveness. To infer the orientation of the cracks, the geometry of the distribution of the seismic events must be investigated (Williams-Stroud & Billingsley 2010). Two types of seismic phenomena have been interpreted as occurring during hydraulic fracturing: wet and dry microseismicity (Maxwell 2014, 2015a, 2015b). In order to correctly interpret the structures formed, it is necessary to distinguish phenomena that are directly created by the flow of fracturing fluid (so-called wet microseismicity). The fracturing operation causes a stress change or stress transfer in the rock mass, resulting in seismic emissions even at large distances from the well (so-called dry microseismicity). It is necessary to distinguish between these two types of events to avoid overestimating the volume of the reservoir, because dry events are not hydraulically connected to pore-pressure induced fracturing.

This paper presents an analysis of microseismic event locations recorded during HF performed from June 9, 2016 to June 18, 2016 in the Wysin-2H/2Hbis horizontal well. The main goal of the paper is to determine the fractures formed by hydraulic fracturing and compare the patterns of these fractures with the direction of regional maximum horizontal stress. The authors developed a novel workflow that uses microseismic event locations to identify linear structures which may be formed by hydraulic fracturing. To minimize the dispersion of the location of events that results from location errors and thus increase the resolution of the cloud of seismic events, a collapsing method (Jones & Stewart 1997) was used. The collapsing procedure produced a more clustered character from scatter event locations. This allows the identification of structures from which seismic emission occurs, such as cracks or fissures in the rock mass. Using the HDBSCAN (Hierarchical Density-Based Spatial Clustering of Applications with Noise) unsupervised machine learning method (Campello et al. 2013), clusters were then

identified inside the seismic events cloud that may correspond to fractures formed in the rock mass. The biggest advantages of this method are its ability to identify noise and find clusters of different shapes, and its lack of a need to assume the number of clusters. The structures formed were compared with the direction of maximum horizontal stress. To identify potential fractures from all delineated clusters, only those that are linear were selected by calculating the elongation coefficient based on the semi-axis length of the point dispersion ellipsoid in the cluster.

In this paper we present the results of the relocation of seismic events after using the collapsing procedure; then, automatic detection of clusters using HDBSCAN is presented. Two seismic event locations (variants before and after applying the collapsing procedure) are compared with the regional stress direction. To validate the locations of microseismic events, a comparative analysis is performed between these two variants of the microseismic cloud, and the estimated probability of a given brittleness index is shown.

## GEOLOGICAL SETTING

Wysin-2H/2Hbis is a horizontal well located in the village of Wysin in the northern part of Poland (see Fig. 1) in the Peri-Baltic Syncline (Zaręba & Danek 2018), situated in the western region of a Lower Paleozoic basin, referred to as the Baltic Basin. This basin is part of the northernmost section of the Polish segment on the Baltica continent, which is also known as the East European Craton (EEC) (see Fig. 2). The geological structure of the Baltic Basin includes a sequence of sediments, ranging from Paleozoic (where shale gas and oil exploration is possible) to Mesozoic (EIA 2013). Figure 3 shows the geological sequence of the study area. About 4 km below the surface, there are Cambrian sandstones and shales overlying Ordovician marly limestone, mudstone, and siltstone, and Silurian shales interbedded with dolomitic limestones (Lopez-Comino et al. 2018). The Pelplin Claystone Formation was hydraulically fractured.

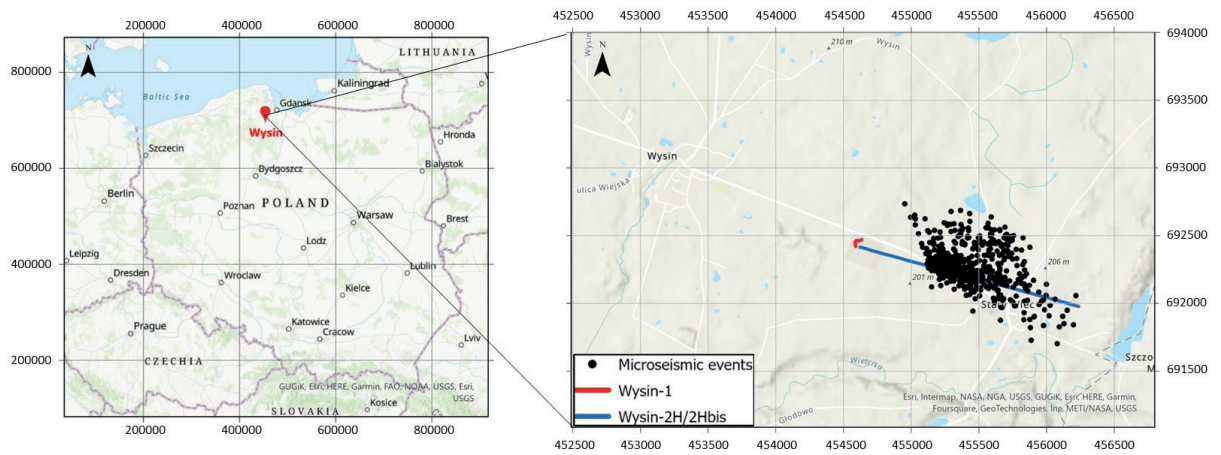


Fig. 1. Location of Wysin village, Wysin-1 and Wysin-2H/2Hbis wells, and microseismic events located during Wysin-2H/2Hbis hydraulic fracturing

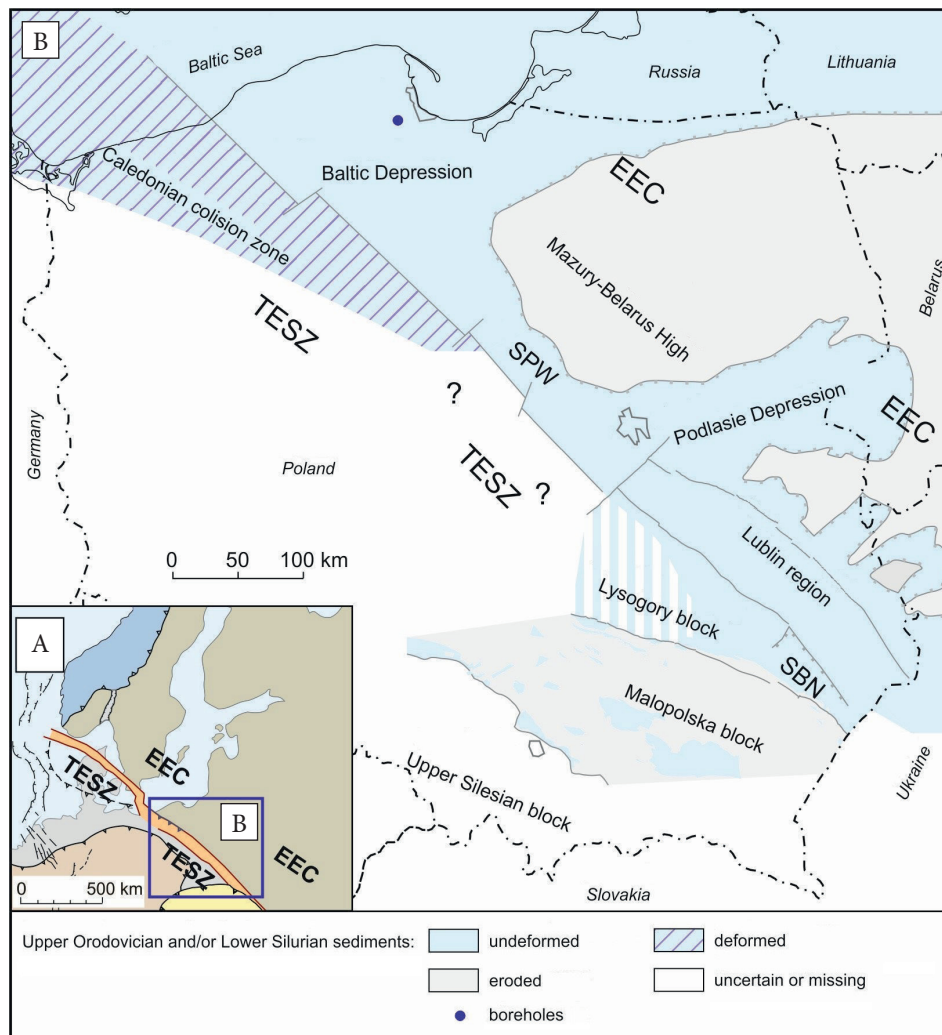


Fig. 2. Location of Lower Paleozoic sedimentary basins and lateral extend of the Upper Ordovician and/or Lower Silurian shale formations: A) western slope of the East European Craton (EEC) with the background of the main tectonic units of the central and northern Europe; B) location of the Lower Paleozoic sedimentary basins in Poland (Poprawa 2010, modified Wandycz 2022); TESZ – Trans-European Suture Zone, SBN – Biłgoraj-Narol zone

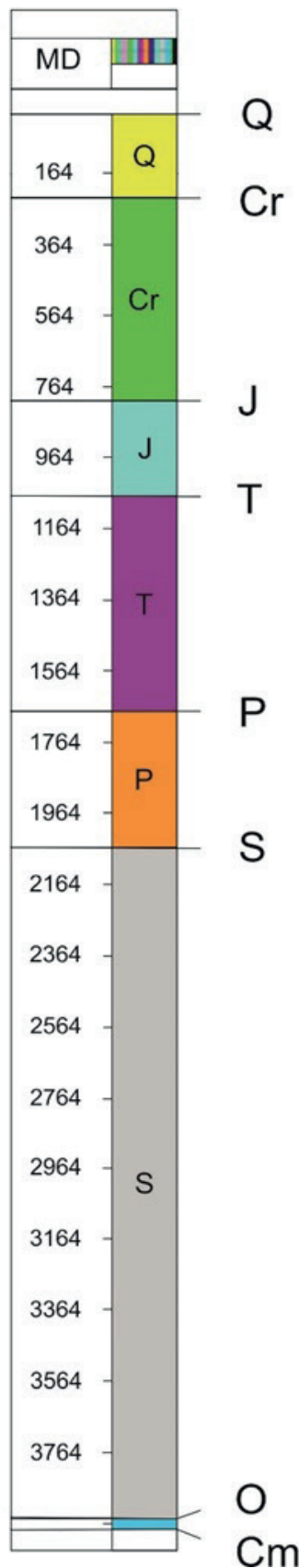


Fig. 3. Stratigraphic profile in Wysin-1 (Wandycz 2022, modified)

## WYSIN-2H/2HBIS HYDRAULIC FRACTURING

The Wysin-2H/2Hbis experiment consisted of eleven stages during which fracking was performed. In each stage, six perforation shots were carried out. During the hydraulic fracturing operation conducted from June 9 to 18, 2016, 565 microseismic events were located. All coordinates are presented in the PUWG1992 (EPSG 2180) system. Figure 4 shows the Wysin-2H/2Hbis injection well, the location of geophones, and localized seismic events in the various stages of fracturing. The 18 triaxial geophones were deployed in the Wysin-1 vertical monitoring well. The fracturing was carried out using the “plug and perf” method. This method is a HF technique that involves isolating fractured parts of the well from the previously fractured zones using plugs after completion of each stage. The stages located in the SE section, which is the deepest part of the horizontal well, were fractured first. The HF process was conducted between 1600 meters (stage 1) and 500 meters (stage 11) from the monitoring array deployed in Wysin-1 well (Wandycz et al. 2019).

Wysin-1 is a vertical hydraulic fracturing monitoring well with a total depth of 4,040 m (Zaręba et al. 2021). In Wysin-1, XRMI images (Pasternacki 2017) were reinterpreted to identify “breakout”-type structures, on the basis of which it was possible to determine the azimuth of maximum horizontal stress. The breakouts are borehole failure features that are characterized by their fixed, perpendicular orientation with respect to the direction of the maximum stress, normal to the axis of the well (Bell & Gough 1979, Zoback 2010). Figure 5 shows the distribution of failure azimuths in the Silurian-Ordovician interval in the Wysin-1 well. The red line indicates the interpreted  $SH_{max}$  direction, whose azimuth is  $150^{\circ}N \pm 15^{\circ}$ , because it is assumed to be perpendicular to the breakout azimuth.

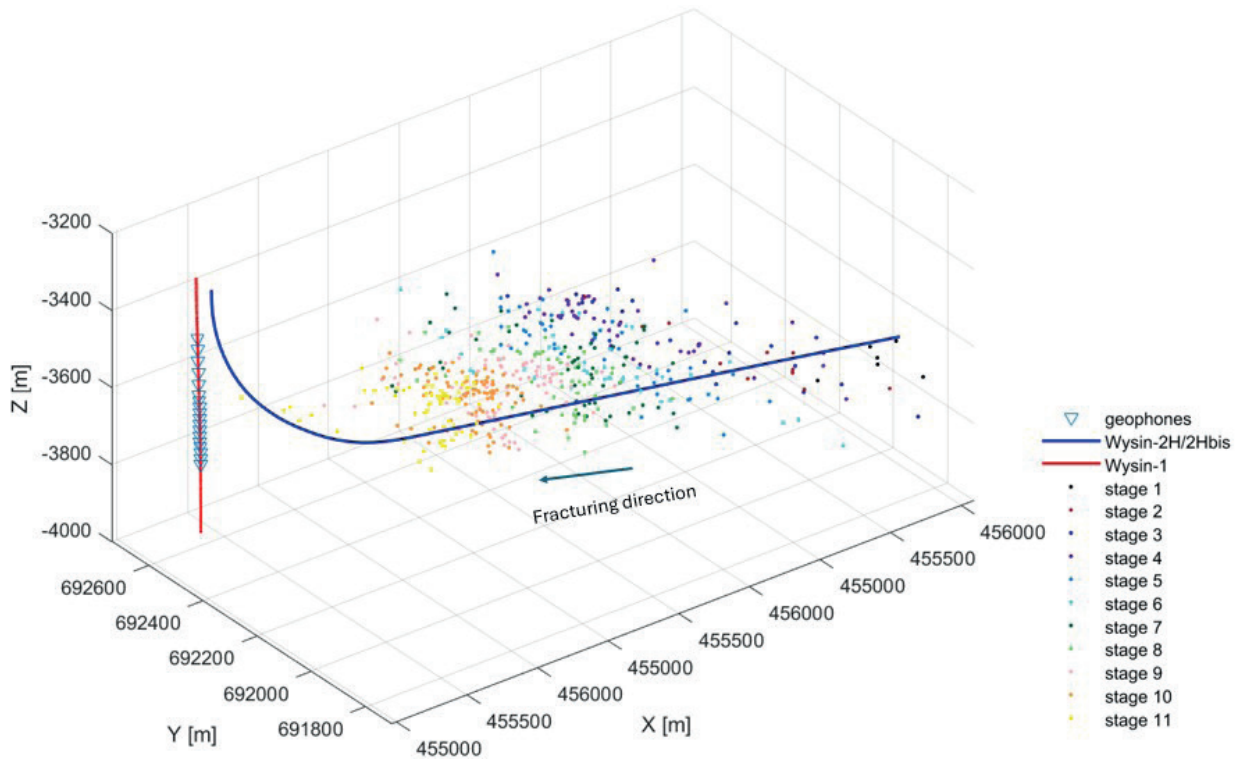


Fig. 4. Location of 18 geophones in the monitoring well, the trajectory of the injection well, and localized seismic events in the various stages of fracturing

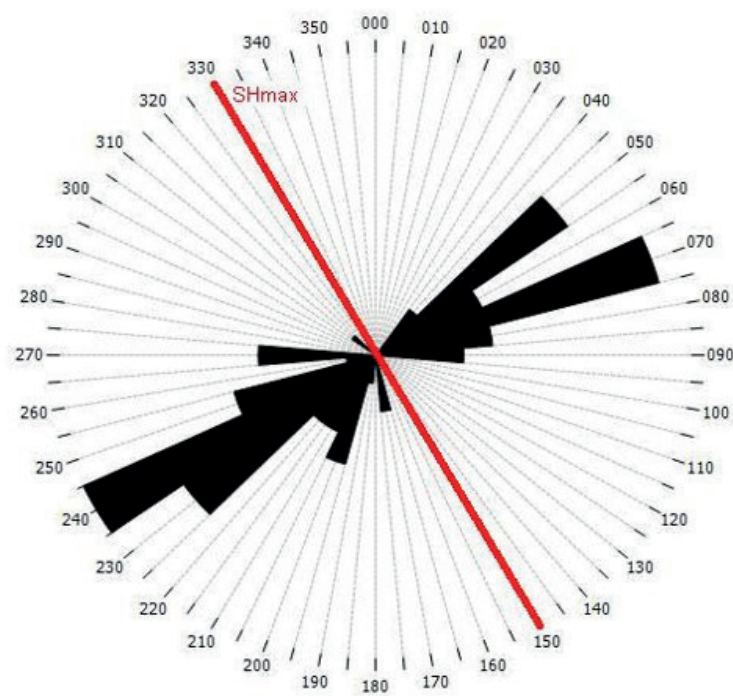


Fig. 5. Distribution of azimuths of breakout features directions in the Silurian-Ordovician interval in Wysin-1 borehole (black); the red line indicates estimated  $SH_{max}$  direction

## METHODS USED TO MAP LINEAR STRUCTURES

To identify structures that could be potential induced hydraulic fractures, the authors proposed a three-step procedure for separating linear structures. Each of the three methods used has an important function in identifying structures. The collapsing method involves minimizing the scattering of events created by localization errors. The HDBSCAN algorithm applied as the second step in the procedure can find groups of points with increased intensity of occurrence in relation to their surroundings. The last step of the procedure, the calculation of scatter ellipsoids for each cluster detected by HDBSCAN, makes it possible to

determine the dominant direction of each structure for comparison with the direction of regional stress. Below is a description of each of the three methods used. A flowchart describing identification of linear structures is presented in Figure 6.

### Collapsing

The locations of seismic events are generally subject to error, which is due to a simplified velocity model or errors in first-break picking. This results in the locations in the seismic cloud being scattered. To discover the pattern of seismicity, the dispersion of events must be minimized. To identify fractures created by hydraulic fracturing, a collapsing method (Jones & Stewart 1997) was used to increase the resolution of the seismic cloud.

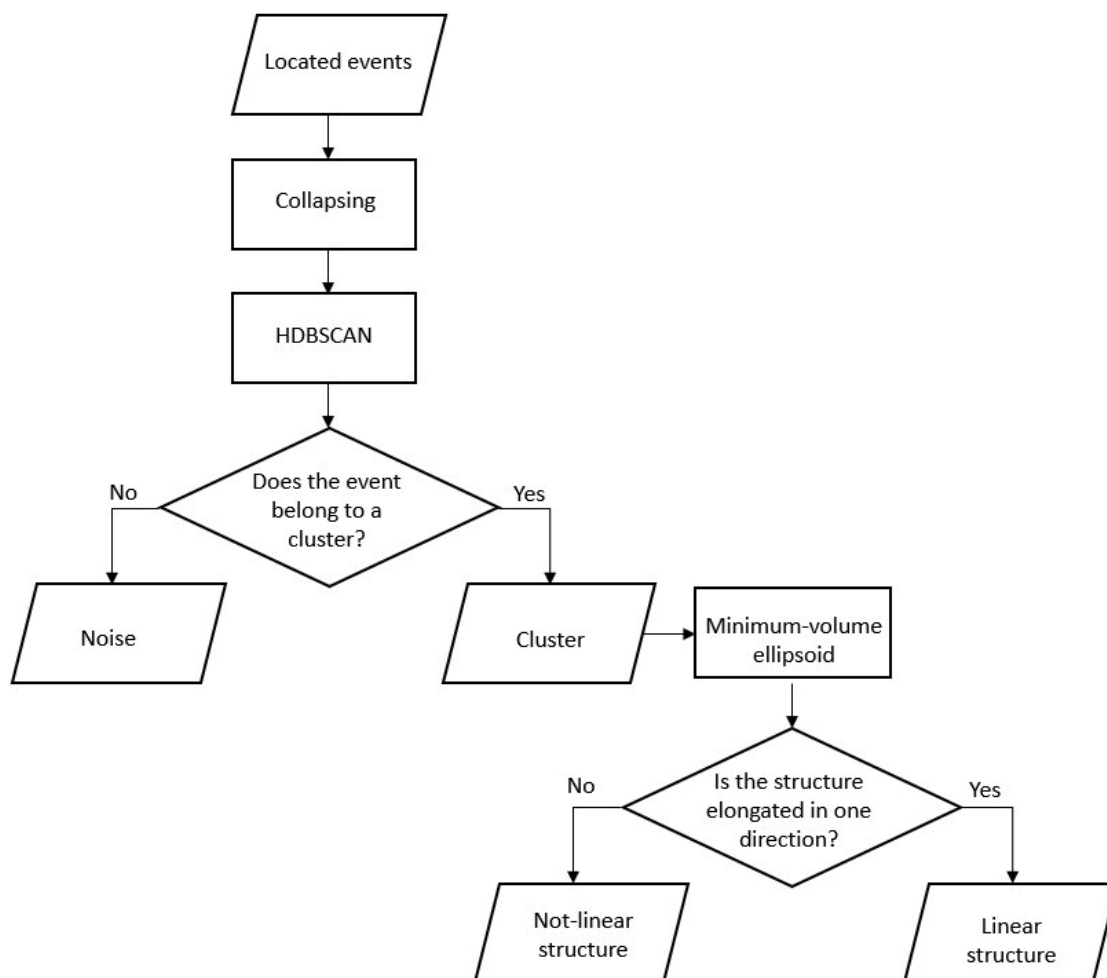


Fig. 6. Flowchart describing linear structures identification

This method enables a more tightly clustered character to be obtained from scattered event locations, thus allowing seismogenic structures to be identified. These structures can be pre-existing features related to tectonic deformation, such as cracks or fissures in the rock mass and associated with seismic emissions.

The first step required in the collapsing method is to determine the error ellipsoid for each seismic event. Under the assumption that errors are random and have a normal distribution, the error ellipsoids can be determined for each event by assuming a statistical significance level. The collapsing algorithm involves the gradual relocation of emission sources in the direction of local centers' densities. The relocation of each event takes place only inside its error ellipsoid. Relocation is performed iteratively until the translation population takes the form of an  $\chi^2$  distribution. This allows new locations of events to be obtained that are equivalent to original locations in a statistical sense. All the details of the algorithm's operations are described in more detail by its authors (Jones & Stewart 1997). While the collapsing method was originally presented for seismological data (Jones & Stewart 1997), it has also been adapted for microseismic data, e.g. (Evans et al. 2005, Leśniak et al. 2020, Węglińska & Leśniak 2021, 2024).

### HDBSCAN algorithm

The HDBSCAN (Campello et al. 2013) automatic cluster detection method was used to identify structures formed or reactivated by hydraulic fracturing. The algorithm was used on the seismic cloud after the collapsing procedure. In this method, like in all algorithms in the group of density-based clustering algorithms, e.g., (Ester et al. 1996, Ankerst et al. 1999), clusters are groups of events whose density is higher than that of points outside clusters (Kriegel et al. 2011). The algorithm identifies so-called cluster cores as seismic sources in whose vicinity (closer than the predetermined epsilon value ( $\epsilon$ ) – the radius of the neighborhood) there is a minimum number of neighboring hypocenters. New hypocenters that are within epsilon distance of any of the core sources are attached to the cluster cores. Hypocenters that are not included in any of the clusters are defined as noise. HDBSCAN has the advantage over other

algorithms in the group of density-based clustering algorithms that it requires only one parameter, which is the minimum number of points forming a cluster. HDBSCAN builds a hierarchy of all possible clusters for different values of neighborhood distance and extracts clusters with the best stability. This method was chosen from other clustering methods because of its ability to identify noise and find clusters of different shapes, and it does not need to assume the number of clusters.

### Mapping linear clusters on the basis of HDBSCAN

To check which clusters identified by HDBSCAN might correspond to linear structures, scatter ellipsoids were calculated, i.e., minimum-volume ellipsoids containing all points in each cluster. This method makes it possible to determine the directions of structures based on the length of the ellipsoid's semi-axis ( $l_1, l_2, l_3$ ). To investigate whether a structure is elongated in one direction, an elongation coefficient ( $E$ ) (Zhou et al. 2019) is calculated on the basis of the lengths of the ellipsoids' semi-axes. Assuming that for each ellipsoid the lengths of the semi-axes fulfill the condition  $l_1 \geq l_2 \geq l_3$ , the elongation coefficient is defined as:

$$E = \frac{l_2}{l_1}.$$

## RESULTS

The first step of the scattering reduction procedure was an evaluation of the error ellipsoids for all hypocenters. The spatial orientation of each ellipsoid is determined by the relative position of the event location and the geophones. The size of the ellipsoid depends on the error in determining the location for the chosen confidence level. The error ellipsoids for the location of the hypocenters of two sample events at a significance level of 99.8% are shown in Figure 7. The collapsing procedure involves iteratively moving events toward the center of gravity inside the ellipsoid until the translation vector achieves a  $\chi^2$  distribution with three degrees of freedom. In each iteration, the Kolmogorov–Smirnov test of the correspondence of the empirical distribution with the theoretical distribution  $\chi^2$  is performed.

In the fourth iteration, the goodness of fit of empirical and theoretical distributions was obtained. The goodness of fit of theoretical and empirical distribution for the first and the last iteration is shown in Figure 8A and B respectively. If, for the entire cloud, the source displacement fulfills this condition, the seismic cloud after relocation statistically corresponds to the original cloud before relocation. The relocated seismic cloud illustrates the spatial distribution of sources allowed within the location error. The relocated seismic cloud after using the collapsing algorithm is shown in Figure 9.

It can be noted that the distribution of collapsed events is more heterogeneous than before the procedure. A clustering of points along linear structures is evident. On the basis of collapsed events, the unsupervised HDBSCAN machine learning method was used to identify clusters that could correspond to induced hydraulic fractures. From the cloud of seismic events, the algorithm extracted clusters with an increased density of events relative to the surroundings. A minimum number of 10 events per cluster was imposed. The number of events needed to form a cluster was chosen based on tests of different values of this parameter.

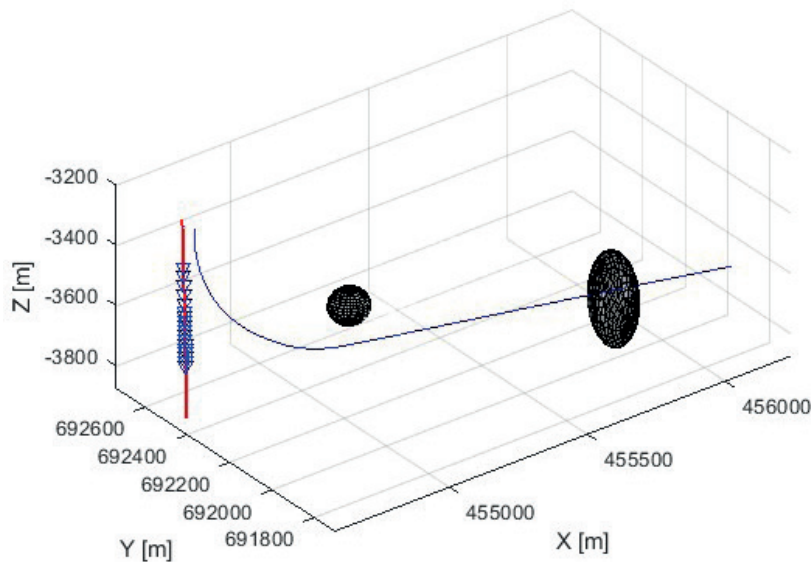


Fig. 7. Error ellipsoids used in the collapsing procedure for the two selected events

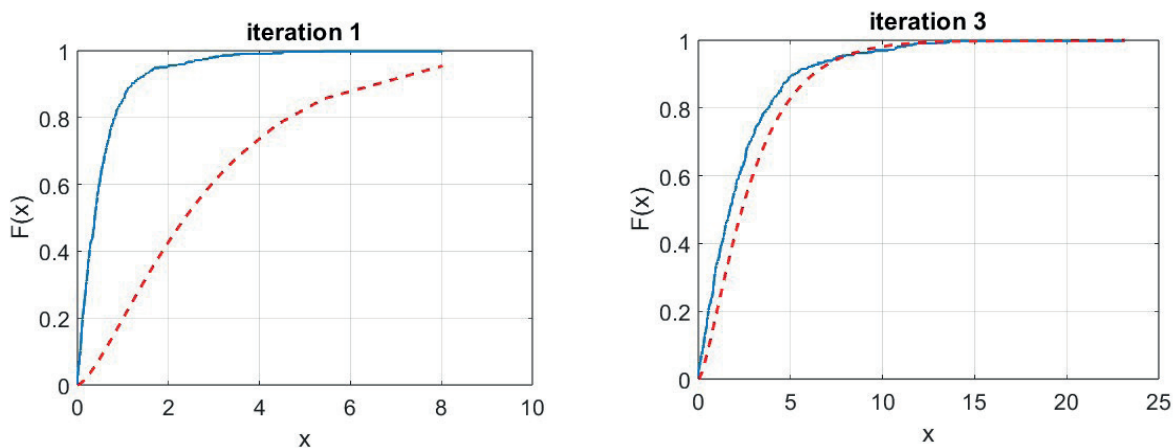


Fig. 8. Comparison of theoretical (blue solid curve) and empirical (red dashed curve) distribution: A) first iteration; B) last iteration

A larger number of events results in mutual aggregation of clusters, while with a smaller number the algorithm did not find linear clusters. The result of the HDBSCAN algorithm is a hierarchical representation of all possible clustering, i.e., for all potential radius values ( $\epsilon$ ). The HDBSCAN hierarchy is presented in Figure 10 in

a simplified form; it shows cluster-wide changes depending on the eps value, and the most stable clusters are outlined in red. HDBSCAN identified 12 clusters and 212 noise points. These clusters have different shapes, dimensions, and population sizes. The population in each cluster is listed in Table 1.

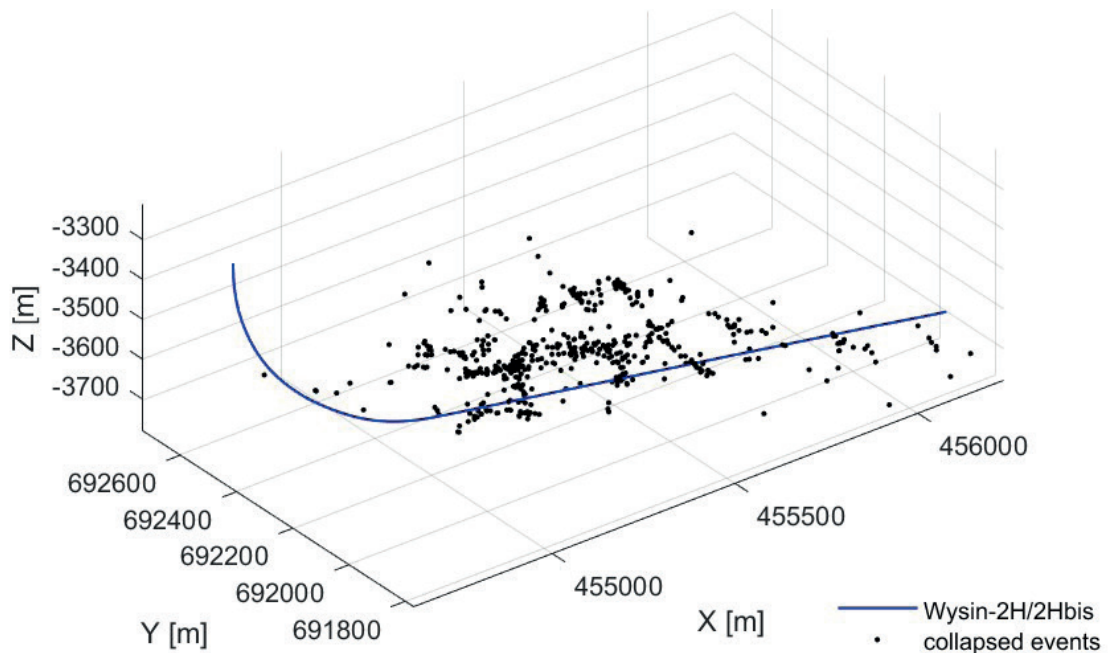


Fig. 9. Result of applying the collapsing method to the microseismic cloud

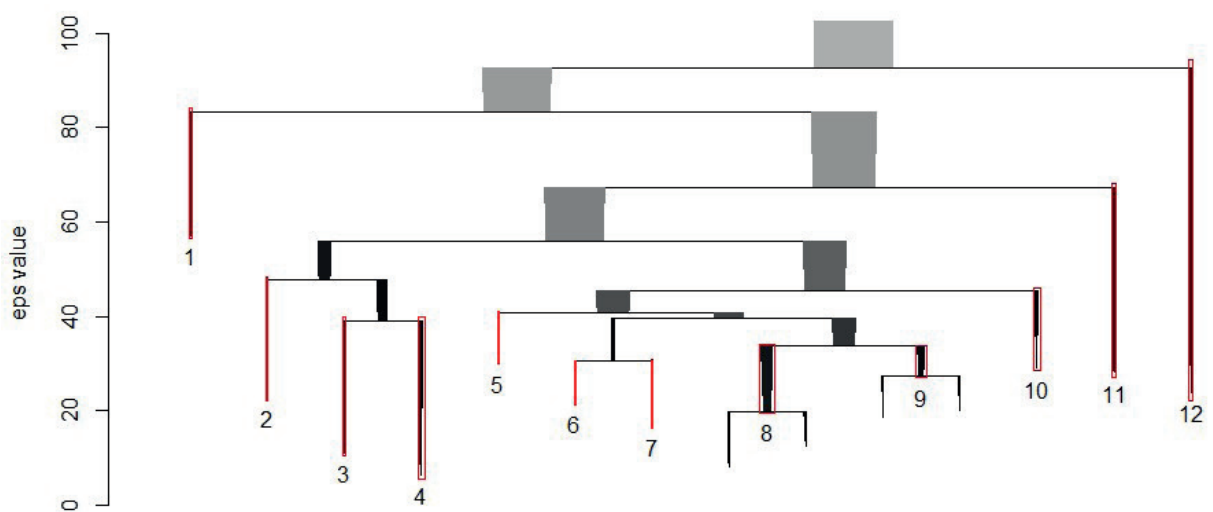


Fig. 10. Cluster hierarchy after applying the HDBSCAN algorithm for all possible radius values. The most stable clusters are outlined in red

**Table 1**  
Events population in each cluster

Cluster number	1	2	3	4	5	6	7	8	9	10	11	12
Number of events	19	14	19	10	23	44	36	11	14	59	91	13

The result of applying the HDBSCAN algorithm to the set of microseismic events after the collapsing procedure is shown in Figure 11. The hypocenters marked in grey represent noise, while the hypocenters in other colors indicate individual clusters. To illustrate the need to apply the collapsing procedure, the Figure 12 shows the result of the detection of clusters in the original seismic cloud using the same parameters as for the collapsed cloud. Clusters identified in this point cloud do not present any obvious structures due to dispersion of events.

In the case of a normal stress regime, the direction of crack development and propagation should follow the direction of  $SH_{max}$  (Zoback 2010) that is observed for the distribution of events in the seismic clouds before (Fig. 13) and after applying the collapsing procedure (Fig. 14). The results after collapsing are characterized by organization

into discrete clusters. The directions of these clusters are more consistent with  $SH_{max}$ . On the other hand, the asymmetry of fracture development, which was not evident in the distribution of events before collapsing, increased significantly. After re-processing, the single-wing nature of the fracture network development in the NNW direction is visible. In particular, this is best seen for later stages of hydraulic fracturing.

The identified clusters are considered as possible structures that developed in the fracturing area. In Figure 15, each identified clusters' scatter ellipsoid is presented, which is a minimum-volume ellipsoid that contains all points in the cluster.

It was assumed that the structure should be elongated in one direction to indicate a potential fracture, i.e., the length of one half-axis must be greater than the other half-axes.

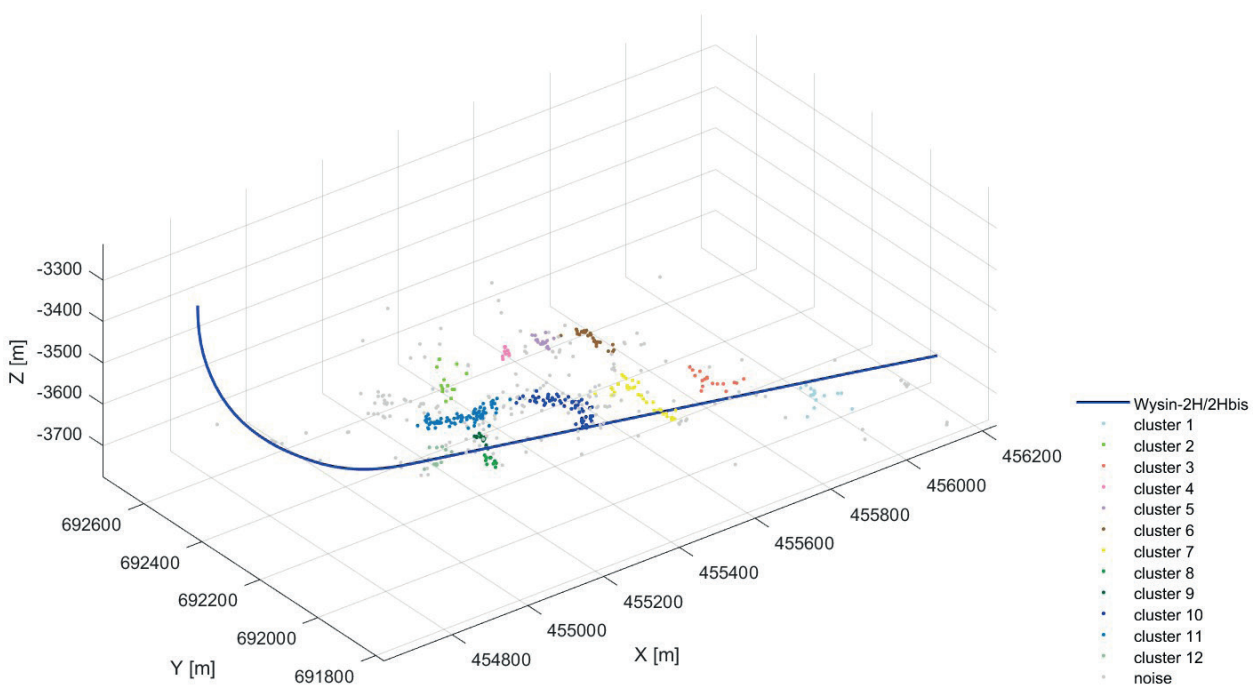


**Fig. 11.** Results of applying the HDBSCAN clustering algorithm to the locations of collapsed events

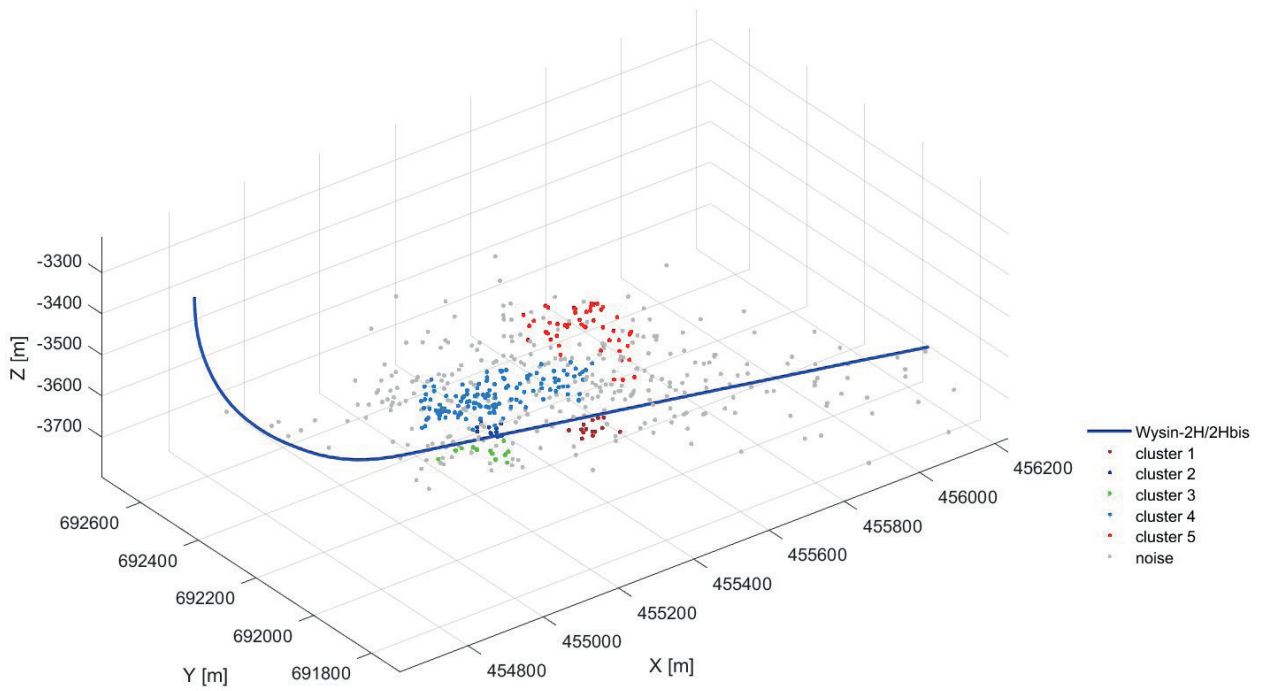


Fig. 12. Results of applying the HDBSCAN clustering algorithm to the original locations of seismic events

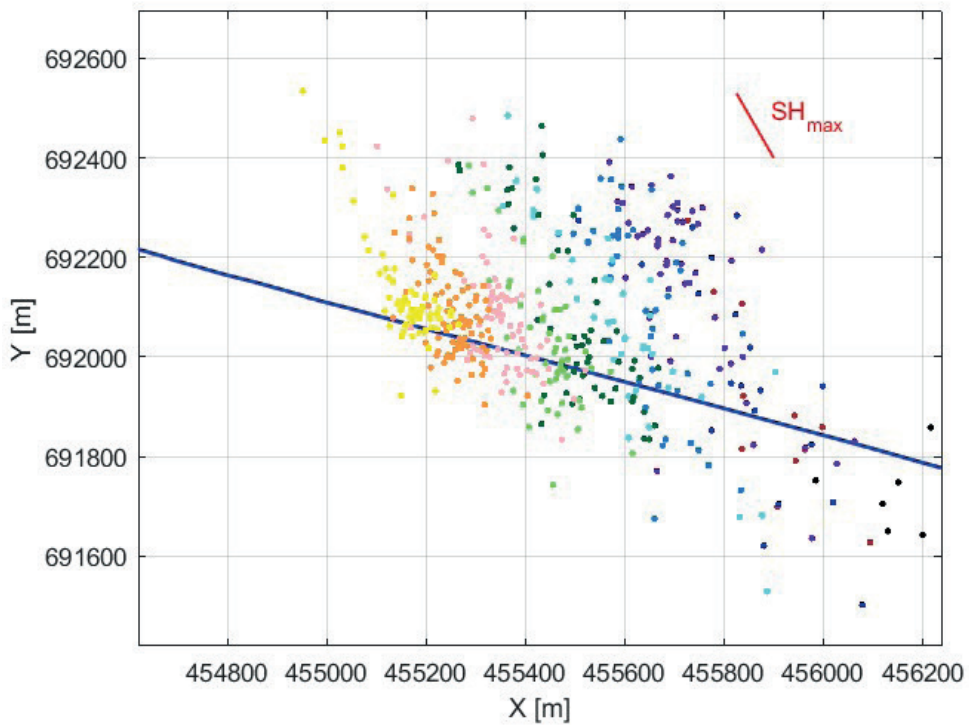


Fig. 13. Distribution of seismic events before the collapsing procedure against the direction of regional horizontal maximum stress. The events are colored by stages

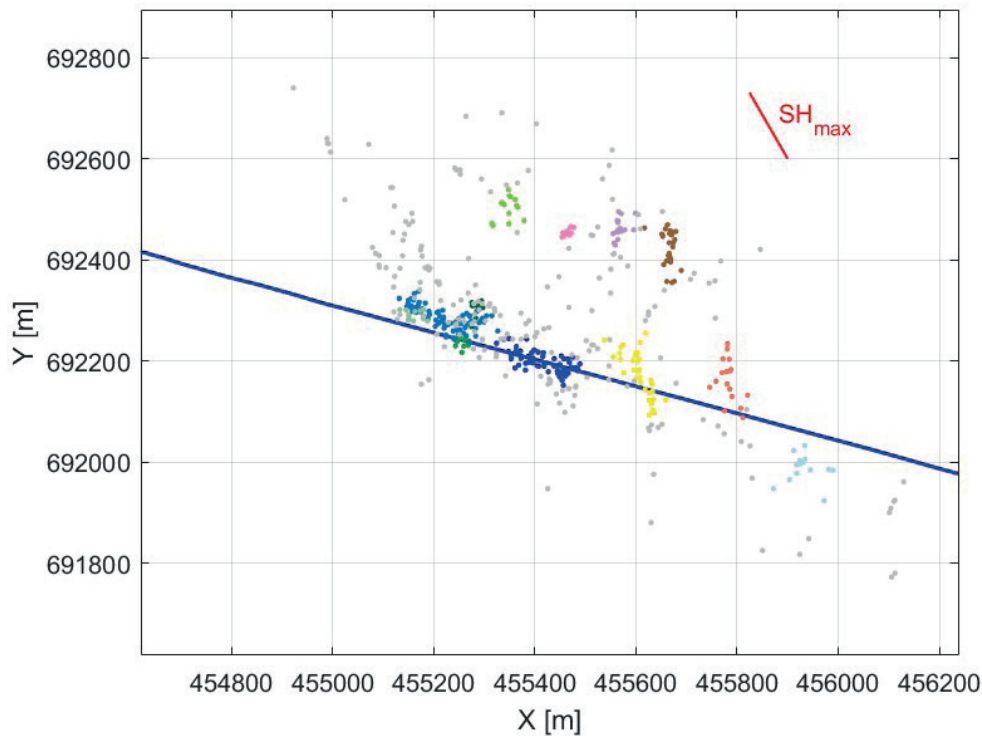


Fig. 14. Distribution of seismic events after the collapsing procedure against the direction of regional horizontal maximum stress. Grey represents points identified as noise; other colors indicate the separated clusters

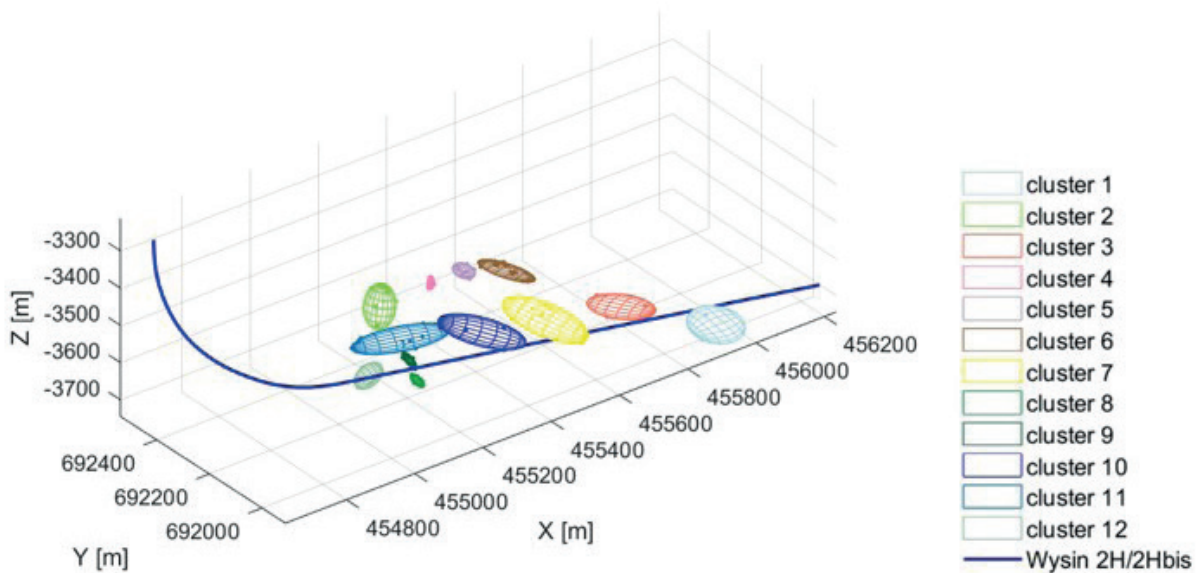


Fig. 15. Minimum-volume ellipsoids containing all events in each cluster

Based on the elongation ratio of the structures (see Table 2), it was concluded that the potential fractures might correspond to cluster numbers 3, 6, 7, 9, 10, 11, 12. To compare the directions of the

ellipsoids for each cluster with the regional maximum horizontal stress, the projection of clusters described by the ellipsoids in the horizontal plane is shown in Figure 16.

**Table 2**  
Lengths of the semi-axes and the elongation coefficient for each ellipsoid

Parameter	Cluster number											
	1	2	3	4	5	6	7	8	9	10	11	12
$l_3$	10.415	37.230	18.368	7.596	4.591	2.970	31.163	3.838	6.354	32.782	25.145	14.166
$l_2$	68.108	44.988	44.991	16.880	25.219	34.711	52.849	18.310	13.890	41.127	43.540	27.353
$l_1$	72.193	55.598	95.766	18.038	42.486	77.680	111.661	21.646	36.948	114.633	120.630	39.010
$E$	0.943	0.809	0.4698	0.936	0.594	0.447	0.473	0.846	0.376	0.359	0.361	0.701

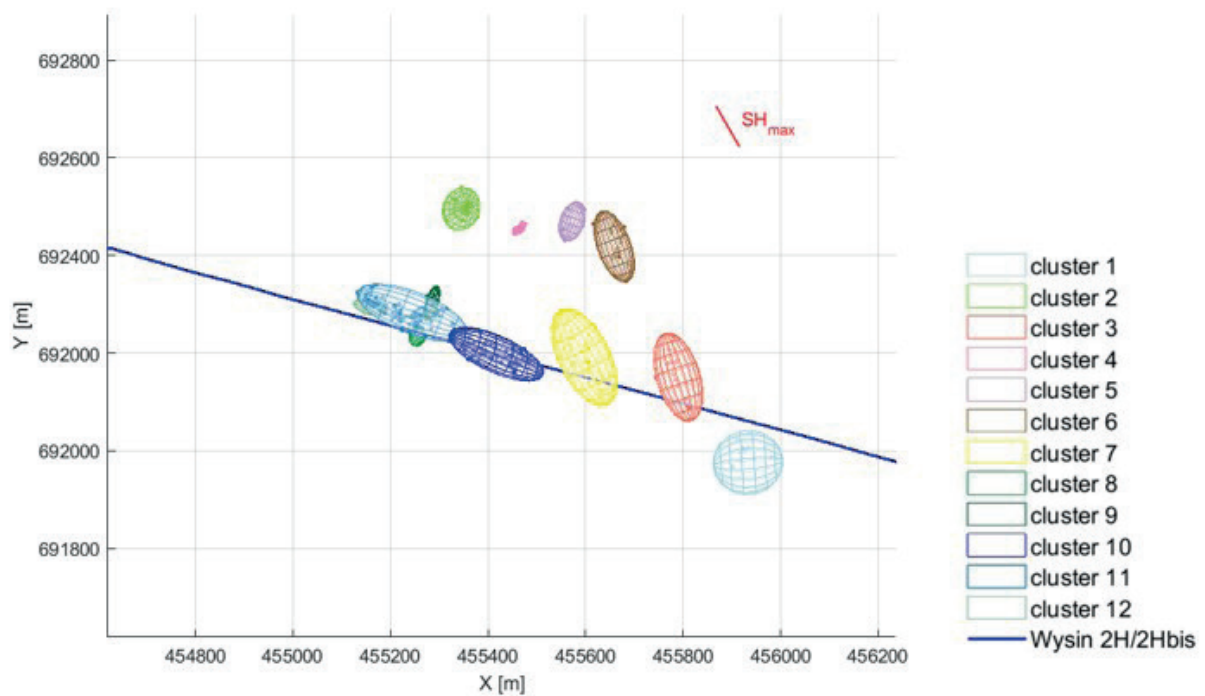


**Fig. 16.** Minimum-volume ellipsoids containing all events in each cluster and the direction of the regional maximum horizontal stress (top view)

## DISCUSSION

The results presented above illustrate an attempt to identify linear structures based on seismic event locations. To perform a validation of our results using the proposed procedure, the results were compared with the 3D seismic image, which has a much higher resolution than seismicity

cloud. The seismic data before and after collapsing were compared against the Wysin 3D seismic survey (a full description of the processing and the interpretation can be found in the unpublished PhD thesis by Pasternacki (2017)). The data were subjected to a standard seismic processing procedure that applied pre-stack time migration. These results made it possible to perform simultaneous

pre-stacking inversion (Pendrel & Dickson 2003), thus the  $Z_p$  (P-wave impedance) and  $Z_s$  (S-wave impedance) attributes could be obtained. A detailed discussion of the operation of simultaneous inversion is presented by Veeken (2007) or Ma (2002). Simultaneous inversion provides information on rock properties, i.e., porosity, water saturation, and lithology. The resolution of the results of such an inversion is higher than in the original seismic image due to the broadening of the spectrum in the higher frequency range based on acoustic profiling measurement data. Simultaneous inversion is used directly to determine the physical properties of rocks based on estimates of their elastic parameters. For surface seismic, these are acoustic impedance ( $Z_p$ ), Poisson's ratio, density ( $\rho$ ), and S-wave impedance ( $Z_s$ ). Density estimation from seismic sections requires the use of a seismic volume containing good-quality seismic reflections from the 40–55° angle range. Due to the limited range of offsets in the data in question, it was not possible to perform seismic inversion to identify the density-defining factor. In recent years, a number of benchmark cross-plots have been developed that estimate the relationship between elastic moduli and lithological formation based on seismic reflection data (Goodway et al. 1997, Perez 2013). Transformation of obtained volumes after prestack seismic inversion  $Z_p$  ( $Z_p = V_p\rho$ , where  $V_p$  is compressional velocity,  $\rho$  is density) and  $Z_s$  ( $Z_s = V_s\rho$ , where  $V_s$  is share wave velocity) to the  $\lambda\rho$ - $\mu\rho$  space (where  $\lambda$  and  $\mu$  are Lamé parameters) allows the partial interpretation of these parameters, even in the present situation, where the pre-stack inversion failed to produce a  $\rho$  volume due to above mentioned quality concerns in reflection angles beyond 40°. LMR ( $\lambda\rho$ - $\mu\rho$ ) analysis provides quantitative information determining lithology, porosity, or reservoir fluid filling (Goodway et al. 1997). The analysis of P-wave impedance with respect to the ratio of P-wave velocity to S-wave velocity can be used to interpret geomechanical parameters. However, interpretation of changes in these parameters is more easily done with LMR analysis.

To test the effectiveness of the collapsing method for localized events in the Wysin-2H/2Hbis experiment, the hypocenters were plotted

against a 3D seismic image. Based on the results of geomechanical parameter calculations for geophysical measurements in the Wysin-1 borehole (Poisson coefficient, Young modulus, geomechanical brittleness coefficient) (Perez & Marfurt 2013), the probability classes of the brittleness index in the LMR parameter domain were determined (Boyd et al. 2010) based on the borehole data. Based on the  $Z_p$  and  $Z_s$  attributes, the probability of a given brittleness index was estimated for the whole space. Figures 17 and 18 show the probability classes of a given range of the brittleness index on a color scale, where 1 indicates rocks with low susceptibility to fracturing, and 4 indicates brittle rocks with higher susceptibility to fracturing. Brittleness maps are shown for 4 depth sections, labeled A-D. Above each map, the depth range of events is shown. The first value refers to the minimum depth of event occurrence, the middle value is the depth cut by the parametric model, and the last is maximum depth of event occurrence. The map labeled A covers the deepest area, while the letter D labels the shallowest surface. Brittleness maps are shown for the original event locations and the relocated event locations at cross-sections of the same depth. It can be noted that for the original locations of events, we are unable to determine whether they occur in more brittle or ductile zones. The distribution of collapsed events, some of which coincide with regions identified as more brittle shows that there is a tendency for rock to fracture preferentially in these areas. In a seismological context, low brittleness index values can also be characterized as areas where less earthquakes will be generated, but more energy accumulation will occur there. In areas with higher brittleness indices, more small earthquakes can be expected. Comparing the two results before and after the collapsing procedure, it can therefore be assumed that the observed asymmetry of later stages of hydraulic fracturing may be related to the transition of the Wysin-2H/2Hbis well to a zone less prone to fracture development. In particular, anomalies “b” and “c” can be interpreted as barriers to fracture development in the south direction, while anomaly “a” is bypassed by microseismic events.

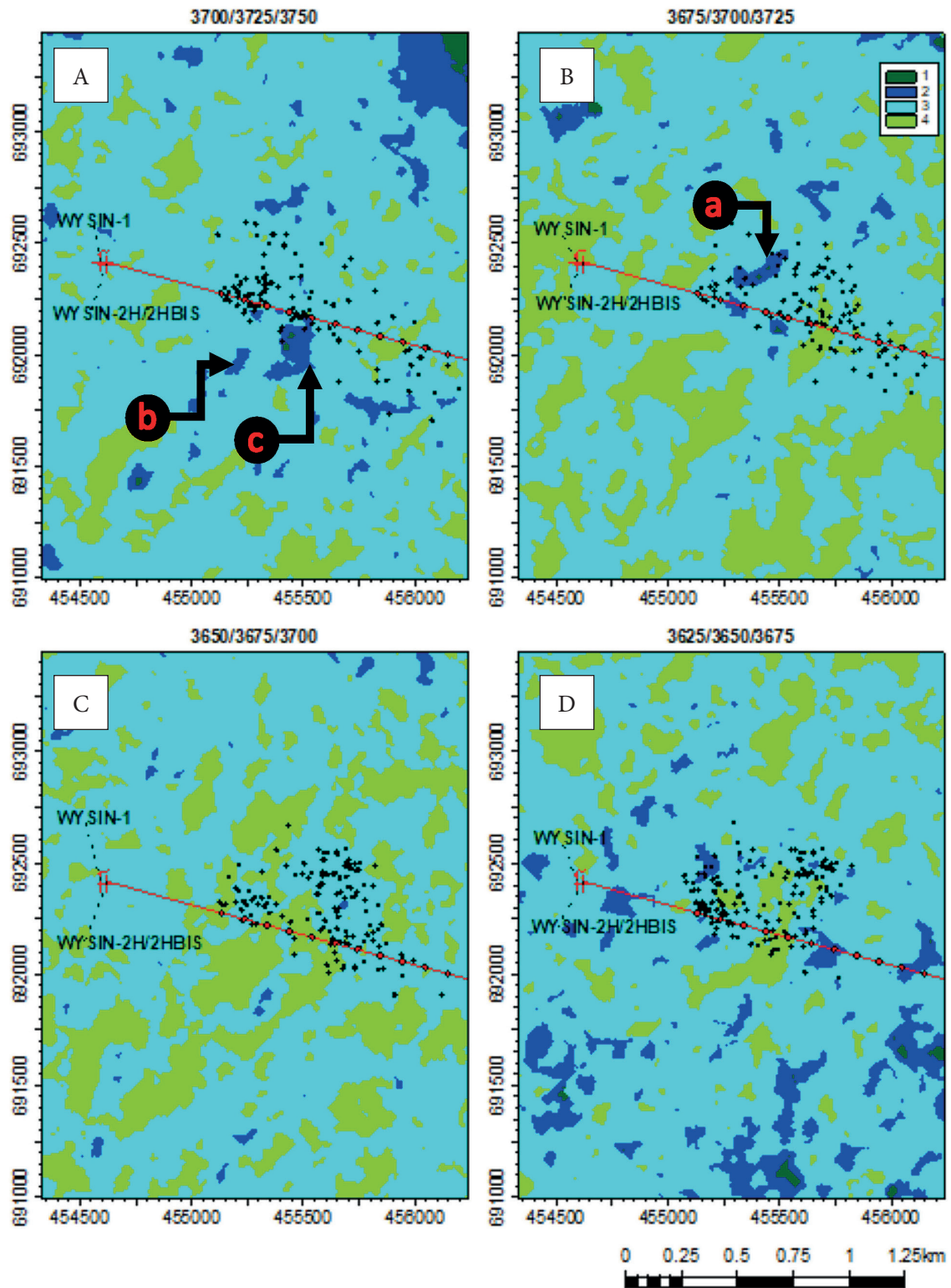
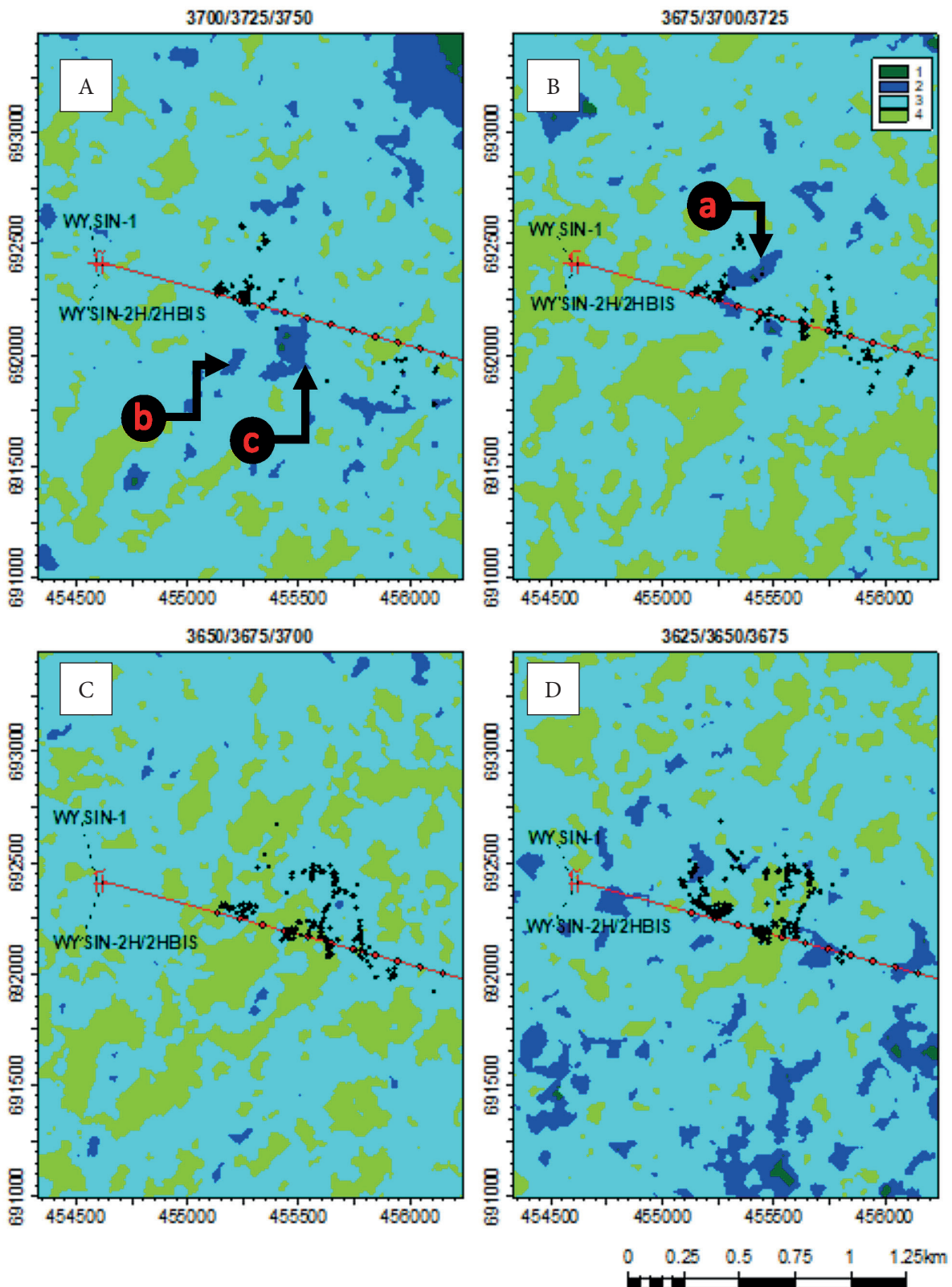


Fig. 17. Probability classes of the brittleness index on microseismic location data before the collapsing procedure: a, b, c – anomalous index values (description in the text). The numerical values above each map refer to minimum depth of event occurrence, depth cut by the parametric model, and maximum depth of event occurrence. Event locations contained within the specific depth interval are shown with black dots. The class 1 indicates rocks with low susceptibility to fracturing, while 4 indicates brittle rocks with higher susceptibility to fracturing



**Fig. 18.** Probability classes of the brittleness index superimposed on microseismic location data after the collapsing procedure: a, b, c – anomalous index values (description in the text). The numerical values above each map refer to minimum depth of event occurrence, depth cut by the parametric model, and maximum depth of event occurrence. Event locations contained within the specific depth interval are shown with black dots. The class 1 indicates rocks with low susceptibility to fracturing, while 4 indicates brittle rocks with higher susceptibility to fracturing

## CONCLUSIONS

Precise imaging of fractures in a scattered seismic cloud is difficult due to event location errors. To identify fractures created during HF, the authors proposed an integrated approach comprising the collapsing method, HDBSCAN clustering, and delineating the linear structures based on the elongation coefficient. These methods were demonstrated on microseismic events located during the fracturing of the Wysin-2H/2Hbis well. The use of the collapsing method made it possible to reduce the dispersion of the cloud of seismic events that results from location errors. Clustering made it possible to separate the areas with increased intensity of events relative to the surrounding area and noise. Determination of the scatter ellipsoid for each separated cluster enabled calculation of the elongation factor, on the basis of which the linear structures were identified. Of the 12 detected clusters, 8 of them can be considered linear structures. The direction determined by the longest semi-axis of the ellipsoid for each structure was contrasted with the direction of maximum horizontal stress. These structures were identified in the earlier stages of fracturing. This approach made it possible to distinguish structures suspected of transporting shale gas. It is important to note that the identified structures do not need to be individual fissures; they can include a series of smaller ones. However, they are located close enough to each other that clustering methods identify them as one large structure. Distinguishing the structures that may be responsible for fluid flow is key to estimating the effectiveness of fracturing. The probability of a given brittleness index was estimated as a technique for recognizing brittle and ductile regions. Comparing the brittleness maps with the seismic cloud before and after collapsing, there appears to be some correlation where the locations after applying the algorithm appeared in more rigid regions. These are areas where we expect more energy release. The results presented in this paper have significant implications for the interpretation of induced seismicity resulting from hydraulic fracturing. Accurate delineation of structures based on the location of microseismic events is key to determining the extent of fracturing. The integrated approach proposed by the authors for fracture identification can be applied to any induced seismicity data.

*This study is part of the project “Appraisal of microseismic monitoring techniques of hydraulic fracturing and development of optimal processing and interpretation methodologies” (SHALEGASMICROS), funded by the Polish National Center for Research and Development within the Program Blue Gas. The authors are grateful to PGNiG SA for generously providing downhole data and seismic data for research purposes. We are very much indebted to the Schlumberger and the Halliburton Landmark Solutions companies for provision of geophysical data interpretation and processing software through the University Software Grants Programs. This research was supported by AGH University of Krakow, Faculty of Geology, Geophysics and Environmental Protection as a part of the statutory project.*

## REFERENCES

- Ankerst M., Breunig M.M., Kriegel H.P. & Sander J., 1999. OPTICS: Ordering points to identify the clustering structure. [in:] *Proceedings of the 1999 ACM SIGMOD International Conference on Management of Data: SIGMOD '99, Philadelphia, PA, USA, June 1–3, 1999*: Vol. 28, Association for Computing Machinery, New York, 49–60. <https://doi.org/10.1145/304182.304187>.
- Bell J.S. & Gough D.I., 1979. Northeast-southwest compressive stress in Alberta evidence from oil wells. *Earth and Planetary Science Letters*, 45(2), 475–482. [https://doi.org/10.1016/0012-821X\(79\)90146-8](https://doi.org/10.1016/0012-821X(79)90146-8).
- Boyd N.K., Cardenas M. & Galarraga M., 2010. Improved reservoir characterization using prestack analyses, Eden Yuturi field, Ecuador. [in:] *SEG Technical Program Expanded Abstracts 2010*, Society of Exploration Geophysicists, 2265–2269. <https://doi.org/10.1190/1.3513301>.
- Campello R.J.G.B., Moulavi D. & Sander J., 2013. Density-based clustering based on hierarchical density estimates. in *advances in knowledge discovery and data mining*. [in:] Pei J., Tseng V.S., Cao L., Motoda H. & Xu G. (eds.), *Advances in Knowledge Discovery and Data Mining: PAKDD 2013*, Lecture Notes in Computer Science, 7819, Springer, Berlin, Heidelberg, 160–172. [https://doi.org/10.1007/978-3-642-37456-2\\_14](https://doi.org/10.1007/978-3-642-37456-2_14).
- Ester M., Kriegel H.P., Sander J. & Xu X., 1996. A density-based algorithm for discovering clusters in large spatial databases with noise. [in:] Simoudis E., Han J. & Fayyad U. (eds.), *KDD'96: Proceedings of the Second International Conference on Knowledge Discovery and Data Mining*, AAAI Press, Portland, Oregon, 226–231.
- Evans K.F., Moriya H., Niitsuma H., Jones R.H., Phillips W.S., Genter A., Sausse J., Jung R. & Baria R., 2005. Microseismicity and permeability enhancement of hydrogeologic structures during massive fluid injections into granite at 3 km depth at Soultz HDR site. *Geophysical Journal International*, 160(1), 388–412. <https://doi.org/10.1111/j.1365-246X.2004.02474.x>.

- Goodway B., Chen T. & Downton J., 1997. Improved AVO fluid detection and lithology discrimination using Lamé petrophysical parameters: “ $\lambda\rho$ ”, “ $\mu\rho$ ”, and “ $\lambda/\mu$  fluid stack”: from P and S inversions. [in:] *SEG Technical Program Expanded Abstracts 1997*, Society of Exploration Geophysicists, 183–186. <https://doi.org/10.1190/1.1885795>.
- Jones R.H. & Stewart R.C., 1997. A method for determining significant structures in a cloud of earthquakes. *Journal of Geophysical Research: Solid Earth*, 102(B4), 8245–8254. <https://doi.org/10.1029/96JB03739>.
- Kriegel H.P., Kröger P., Sander J. & Zimek A., 2011. Density-based clustering. *WIRES Data Mining and Knowledge Discovery*, 1(3), 231–240. <https://doi.org/10.1002/widm.30>.
- Leśniak A., Śledź E. & Mirek K., 2020. Detailed recognition of seismogenic structures activated during underground coal mining: A case study from Bobrek Mine, Poland. *Energies*, 13(18), 4622. <https://doi.org/10.3390/en13184622>.
- Lopez-Comino J.A., Cesca S., Jaroslowski J., Montcoudiol N., Heimann S., Dahm T., Lasocki S., Gunning A., Capuano P. & Ellsworth W.L., 2018. Induced seismicity response of hydraulic fracturing: results of a multidisciplinary monitoring at the Wysin site, Poland. *Scientific Reports*, 8, 8653. <https://doi.org/10.1038/s41598-018-26970-9>.
- Ma X.Q., 2002. Simultaneous inversion of prestack seismic data for rock properties using simulated annealing. *Geophysics*, 67, 1877–1885. <https://doi.org/10.1190/1.1527087>.
- Maxwell S.C., 2013. Unintentional seismicity induced by hydraulic fracturing. *CSEG Recorder*, 38(08), 40–49.
- Maxwell S.C., 2014. *Microseismic Imaging of Hydraulic Fracturing: Improved Engineering of Unconventional Shale Reservoirs*. Distinguished Instructor Series, 17, Society of Exploration Geophysicists. <https://doi.org/10.1190/1.9781560803164>.
- Maxwell S.C., Mack M., Zhang F., Chorney D., Goodfellow S.D. & Grob M., 2015a. Differentiating wet and dry microseismic events induced during hydraulic fracturing. [in:] *SPE Unconventional Resources Technology Conference 2015: San Antonio, Texas, USA, 20–22 July 2015*, <https://doi.org/10.15530/urtec-2015-2154344>.
- Maxwell S.C., Chorney D. & Goodfellow S.D. 2015b. Microseismic geomechanics of hydraulic-fracture networks: Insights into mechanisms of microseismic sources. *The Leading Edge*, 34(8), 904–910. <https://doi.org/10.1190/tle34080904.1>.
- Pasternacki A., 2017. *Ocena efektywności procesu szczelinowania hydraulicznego w eksploatacji gazu ziemnego z łupków ilastych na podstawie badań mikrosejsmicznych [Appraisal of hydraulic fracturing effectiveness in the shale gas exploration based on microseismic monitoring]*. Akademia Górniczo-Hutnicza, Kraków [PhD thesis, unpublished].
- Pendrel J. & Dickson T., 2003. Simultaneous AVO inversion to P impedance and Vp/Vs. [in:] *CSEG Annual Meeting Abstracts 2003*, Canadian Society of Petroleum Geologists, Calgary, 417S0131. <https://old.cseg.ca/assets/files/resources/abstracts/2003/417S0131.pdf>.
- Perez R., 2013. Brittleness estimation from seismic measurements in unconventional reservoirs: Application to the Barnett Shale. [in:] *SEG Technical Program Expanded Abstracts 2013*, University of Oklahoma, Oklahoma, 2258–2263. <https://doi.org/10.1190/segam2013-0006.1>.
- Perez R. & Marfurt K., 2013. *Calibration of brittleness to elastic rock properties via mineralogy logs in unconventional reservoirs* [conference poster]. AAPG International Conference and Exhibition. [https://www.searchanddiscovery.com/documents/2013/41237perez/ndx\\_perez.pdf](https://www.searchanddiscovery.com/documents/2013/41237perez/ndx_perez.pdf).
- Poprawa P., 2010. Potencjał występowania złóż gazu ziemnego w łupkach dolnego paleozoiku w basenie bałtyckim i lubelsko-podlaskim [Shale gas potential of the Lower Palaeozoic complex in the Baltic and Lublin-Podlasie basins]. *Przegląd Geologiczny*, 58(3), 226–249.
- U.S. Energy Information Administration (EIA), 2013. *Technically recoverable shale oil and shale gas resources: An assessment of 137 shale formations in 41 countries outside the United States*. U.S. Department of Energy, Washington. <https://www.eia.gov/analysis/studies/worldshalegas/pdf/overview.pdf> [access: 18.04.2024].
- Veeken P.C.H., 2007. *Seismic Stratigraphy, Basin Analysis and Reservoir Characterisation*. Elsevier, Amsterdam.
- Wandycz P., 2022. *Wyznaczenie współczynnika dobroci Q na podstawie zdarzeń mikrosejsmicznych indukowanych podczas procesu szczelinowania hydraulicznego oraz ocena możliwości jego wykorzystania w przetwarzaniu danych mikrosejsmicznych [Determination of the quality factor Q from microseismic events induced during the hydraulic fracturing process and evaluation of its applicability in microseismic data processing]*. Akademia Górniczo-Hutnicza, Kraków [PhD thesis, unpublished].
- Wandycz P., Święch L., Eisner L., Pasternacki A., Wcisło M. & Maćkowski T., 2019. Estimation of the quality factor based on the microseismicity recordings from Northern Poland. *Acta Geophysica*, 67, 2005–2014. <https://doi.org/10.1007/s11600-019-00362-7>.
- Węglińska E. & Leśniak A., 2021. Induced seismicity and detailed fracture mapping as tools for evaluating HDR Reservoir Volume. *Energies*, 14(9), 2593. <https://doi.org/10.3390/en14092593>.
- Węglińska E. & Leśniak A., 2024. A novel approach to identifying seismogenic structures and estimating reservoir volume based on synthetic cloud of seismicity induced by hydraulic fracturing. *Acta Geodaetica et Geophysica*. <https://doi.org/10.1007/s40328-024-00442-1>.
- Williams-Stroud S. & Billingsley R.L., 2010. Techniques to estimate fracture effectiveness when mapping low-magnitude microseismicity. [in:] *SEG Technical Program Expanded Abstracts 2010*, Society of Exploration Geophysicists, Houston, 2075–2079. <https://doi.org/10.1190/1.3513253>.
- Zaręba M. & Danek T., 2018. VSP polarization angles determination: Wysin-1 processing case study. *Acta Geophysica*, 66, 1047–1062. <https://doi.org/10.1007/s11600-018-0200-8>.
- Zaręba M., Danek T. & Stefaniuk M., 2021. P-wave-only inversion of challenging walkaway VSP data for detailed estimation of local anisotropy and reservoir parameters: A case study of seismic processing in Northern Poland. *Energies*, 14(8), 2061. <https://doi.org/10.3390/en14082061>.
- Zhou C., Zhang M., Li Y., Lu J. & Chen J., 2019. Influence of particle shape on aggregate mixture’s performance: DEM results. *Road Materials and Pavement Design*, 20(2), 399–413. <https://doi.org/10.1080/14680629.2017.1396236>.
- Zoback M.D., 2010. *Reservoir Geomechanics*. Cambridge University Press, Cambridge.